Effect of Topology on the Adhesive Forces Between Electrospun Polymer Fibers Using a T-peel Test

Florencia Montini Ballarin,[1,2] Todd A. Blackledge,[3] Nicole L. Capitos Davis,[4] Patricia M. Frontini,[2] Gustavo A. Abraham,[2] Shing-Chung Wong[1]

[1] *Department of Mechanical Engineering, The University of Akron, Akron, Ohio 44325-3903*

[2] *Research Institute for Materials Science and Technology (INTEMA, UNMdP-CONICET), B7608FDQ, Mar del Plata, Buenos Aires, Argentina*

[3] *Department of Biology and Integrated Bioscience Program, University of Akron, Akron, Ohio 44325-3908*

[4] *Center for Research and Technology, Bridgestone Americas, Akron, Ohio 44301*

Electrospinning provides an effective methodology to obtain high aspect ratio polymer fibers for biomimetic applications. In this article, we evaluate the effect of topology on adhesion between aligned fibers. Polycaprolactone is electrospun using two different setups: (i) a tip collector and (ii) a flat collector. The tip collector enables the fibers to self-align. When a fiber reaches the tip collector, the next fiber is repelled by the charge they carry, forcing the fibers to deposit in a parallel arrangement. The flat collector allows the fibers to deposit at random. The adhesion between the fiber mats is measured using a T-peel test. Adhesion strength (758.7 ± 211.7 kPa) changes marginally with the peeling rate and applied pressure on the membranes. Aligned fibers exhibit higher adhesion strength between the membranes in comparison to randomly oriented nonwovens (613.1 ± 79.9 kPa). The estimated Johnson–Kendall–Roberts contact energy (83.1 ± 32.5 mJ/m^2) is consistent with the range of van der Waals adhesion forces. This work shows how the adhesion between two polymer membranes can be modulated by surface topology, based on a T-peel testing setup. POLYM. ENG. SCI., 00:000–000, 2013. © 2013 Society of Plastics Engineers

INTRODUCTION

The ability to fabricate synthetic and flexible polymers mimicking naturally occurring phenomena is of continued interest. For instance, the adhesion based on van der Waals (vdW) forces by insect tarsal pads and gecko toes inspired a flurry of research activities to produce synthetic dry adhesives [1–11]. Contact area per unit volume plays an important role in these systems in influencing the fibril adhesion strength. The adhesion force for a given contact area becomes stronger as the total contact splits into smaller contact structures. This contact splitting efficiency can be evaluated by contact mechanics [12–14]. Apart from the effect of contact area, previous work demonstrated the importance of surface topology on adhesion [15–21]. Within this context, Greiner et al. shows that an elastic band-like structure is one of the most efficient topologies for constructing hierarchical artificial adhesives [19]. Gecko's toe pad exhibits numerous free-standing and flexible fibrous structures which can penetrate into surface asperities for enhanced splitting contacts with the adherend. Once the adhesive and the adherend are in proximity, there are molecular interactions such as the vdW forces involved in the bond, which contribute significantly to the bond strength arising from millions of contact points of nanofibers. By demonstrating the effect of topology on membrane adhesion, using a T-peel testing geometry, we will develop fruitful insights into making use of flexible fibers for adhesive applications. A better understanding of the influence of membrane topology on adhesion strength is thus clearly needed.

Electrospinning provides a versatile tool for creating hierarchical structures with a high aspect ratios [22, 23], capable of supporting significant loads (Fig. 1). The use of different collector setups produces membranes with different sizes, shapes, and orientations of fibers, making it

Correspondence to: Shing-Chung Wong; e-mail: swong@uakron.edu
Contract grant sponsor: National Science Foundation under a CAREER Award CMMI; contract grant number: 0746703; contract grant sponsor: Argentinean National Agency of Scientific and Technological Promotion; contract grant number: PICT 0448.
DOI 10.1002/pen.23474
Published online in Wiley Online Library (wileyonlinelibrary.com).

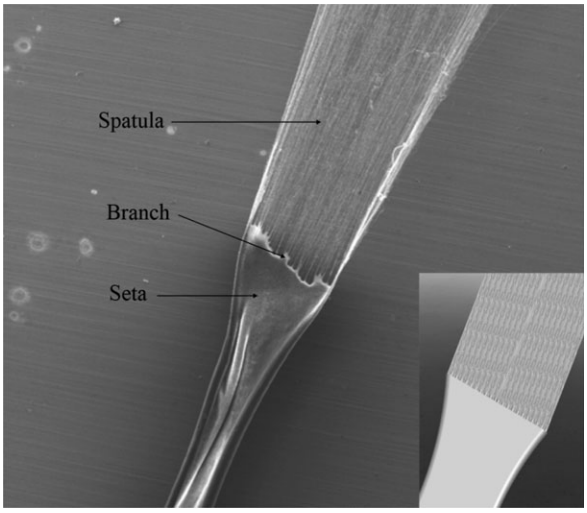

FIG. 1. SEM micrograph of hierarchical structure made by electrospinning of PCL [24]. Insert: schematic diagram.

possible to produce bio-inspired adhesives [25–28]. Presently, the mechanisms of adhesion of electrospun fiber membranes are poorly understood [10, 11, 29]. However, electrospun materials present numerous local contact points that could mimic the splitting efficiency of biological adhesives.

Polycaprolactone (PCL) is a biodegradable polyester commonly used in biomedical applications, such as drug delivery systems, tissue engineering, and biomedical devices [30, 31]. PCL is a hydrophobic aliphatic polyester that exhibits semicrystalline structures and good electro-spinability. The adhesion of PCL membranes is the focus in this article because of the material's suitability for so many applications.

The peel test is a simple and commonly used method to quantify bulk adhesion between two surfaces [32–39]. A fracture mechanics interpretation of the adhesive's detachment is used to obtain and compare the adhesive strength and energy of specimens tested in different peel configurations [33–39]. Kaelble re-analyzed the peel test, increasing confidence when testing two flexible adhering surfaces [40]. The T-peel configuration is mainly applied to measure adhesion between flexible adherents, including polymer/polymer surfaces. It therefore presents an attractive way to address the adhesion properties of electrospun polymers.

In this article, we measure the adhesion between electrospun PCL membranes, constructed from either band-like or non-oriented fibers, using a T-peel test. Two electrospinning setups are used to obtain random and well-aligned nanofibrous membranes: (i) a tip collector [41] and (ii) a flat grounded collector. The mechanism of adhesion between the nanofibrous membranes is evaluated by adsorption theory and classical Johnson–Kendall–Roberts (JKR) contact mechanics. We compare the effects of the peeling rate, the applied pressure, and the orientation of the nanofibers on the adhesive strength to understand how nanoscale topology influences adhesion.

EXPERIMENTAL WORK

Materials

PCL (M_n = 80,000) was purchased from Sigma-Aldrich (CAS = 24980-41-4), and used as received. Reagent grade *N,N*-dimethylformamide (DMF), dichloromethane (DCM), and tetrahydrofuran (THF) were obtained from Fisher, Acros, and EMD Chemicals, respectively.

Electrospinning Process

Two different electrospinning setups are used to obtain aligned and random orientations of the polymer fibers: (i) a tip collector (a wire grounded electrode inside a wooden board) [41] and (ii) a grounded collector plate, respectively. A 22-gauge needle (0.508 mm in internal diameter) and a high-voltage power supply (Gamma High Voltage Research, Ormond Beach, FL) are used (Fig. 2). In order to obtain a bead-free fibrous membrane, intrinsic solution properties (concentration and solvent composition) and setup parameters are first optimized. For the tip collector setup, a wide range of PCL solutions, from 9 to 14% wt/vol (A09DT-A14DT samples in Table 1), is used. This range is selected in order to obtain the critical concentration at which the fibers will be aligned and bead-free. The voltage and the distances (L, $h1$, and $h2$) used in the process are selected based on the best response to alignment. The solutions are listed in Table 1. In this three sequence

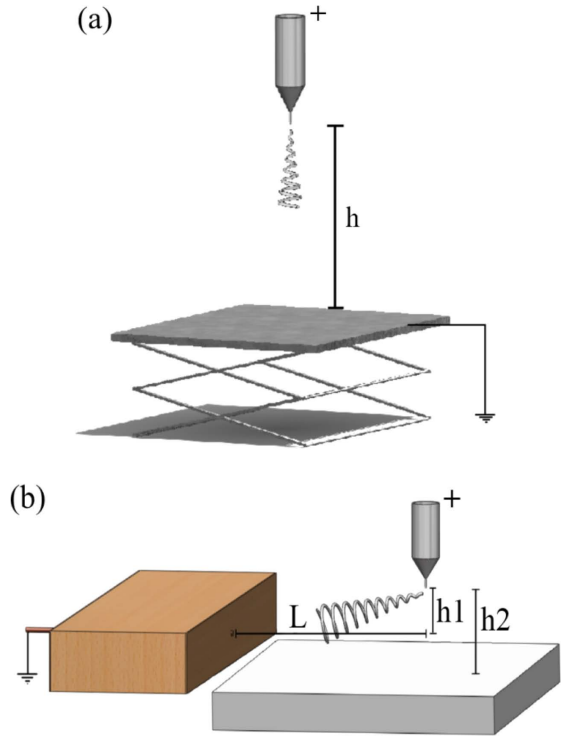

FIG. 2. Schematics for (a) random mesh collection; h = flat collector-needle distance; and (b) tip collector electrospinning setup; $h1$ = tip collector-needle vertical distance, L = tip collector-needle horizontal distance, $h2$ = collector plate-needle distance. [Color figure can be viewed in the online issue, which is available at wileyonlinelibrary.com.]

DOI 10.1002/pen

TABLE 1. Random and aligned electrospun fiber samples.

Sample	Solution concentration and solvent mixture	Fiber morphology
A09DT	9% wt/vol in DMF:THF = 1:1 by volume	No fibers
A10DT	10% wt/vol in DMF:THF = 1:1 by volume	No fibers
A11DT	11% wt/vol in DMF:THF = 1:1 by volume	No fibers
A12DT	12% wt/vol in DMF:THF = 1:1 by volume	Random fibers (angle standard deviation = 51.0°)
A13DT	13% wt/vol in DMF:THF = 1:1 by volume	Poorly aligned fibers (angle standard deviation = 6.7°)
A14DT	14% wt/vol in DMF:THF = 1:1 by volume	Aligned fibers (angle standard deviation = 5.8°)
R12DD	12% wt/vol in DMF:DCM = 1:0.7 by volume	Random fibers (angle standard deviation = 43.0°)
R13DD	13 % wt/vol in DMF:DCM = 1:0.7 by volume	Random fibers (angle standard deviation = 60.4°)
R12DT	12% wt/vol in DMF:THF = 1:1 by volume	No fibers
R13DT	13% wt/vol in DMF:THF = 1:1 by volume	Random fibers (angle standard deviation = 52.0°)

code, the first letter (A or R) indicates the fiber morphology (aligned or random); the following two numbers indicate the solution concentrations (%wt/vol); and the last two letters denote the solvent mixture (DT = DMF:THF and DD = DMF:DMC).

To isolate the influence of topology (aligned vs. random) on adhesion strength, membranes with similar fiber diameters are necessary. Hence, in order to produce random bead-free fibrous membranes with approximately the same mean diameter as that of the aligned fibers, various PCL solutions with different solvents and concentrations are first explored. The concentrations include 12 and 13% wt/vol in a solvent mixture of DMF:DCM, which is equivalent to 1:0.7 by volume (R12DD and R13DD samples in Table 1), and 12 and 13% wt/vol in a solvent mixture of DMF:THF, which is equivalent to 1:1 by volume (R12DT and R13DT samples in Table 1). The setup parameters are varied as conditions warrant. The electrospun fibers range from 200 to 800 nm in diameter.

Sample Preparation

After the optimal electrospinning parameters are established to obtain aligned and random bead-free nanofibers, the fibers are then collected for adhesion studies. According to each solution performance the A14DT is selected to prepare the aligned fibrous samples (see subsection "Electrospinning" under Results and Discussion). Electrospinning is conducted with $h1$ set at a vertical distance of 3.5 cm, L of 12 cm, $h2$ of 5.5 cm, and an applied voltage of 20 kV. The fiber collection is carried out for 10 h to assure enough thickness to perform the peel tests.

For the random fiber mat, the R12DD solution is used. The setup parameters are: $h = 15$ cm and an applied voltage = 12 kV. The nanofibrous membranes are glued on the borders to an aluminum foil that supports the membrane during testing.

Morphological Characterization

The electrospun membranes are observed in a Hitachi S-4800 scanning electron microscope (SEM) before and after mechanical testing. Samples are mounted on the aluminum stub using copper double sided adhesive tape, sputter coated with silver in an argon-purged chamber evacuated to 500 mTorr, and examined using SEM with an accelerating voltage of 25 kV. The micrographs are processed with image processing software (Image Pro Plus) to measure the diameter and orientation of the nanofibers. Approximately, 100 nanofibers per sample are measured in order to obtain a meaningful statistical value. Some samples are also examined after testing. Two regions, one from the beginning of the detaching area and the other from the stable peeling zone, are observed.

Peel Test

A T-peel test configuration is used to evaluate the adhesion of the nanofibers between each other (Fig. 3). Samples consist of 5 mm × 50 mm of aligned and random nanofibrous membranes attached to aluminum substrates. A 750 g plastic cylinder is first rolled over the samples to apply a uniform pressure. Tests are conducted in a Nano Bionix® tensile tester (MTS Systems Corp—now Agilent Technologies, Oak Ridge, TN), with a load resolution of 2 μN and an extension resolution of 1 μm. The effects of peeling rate and applied pressure on the peel force are studied only for aligned membranes. The applied pressure was changed by varying the numbers of times the plastic cylinder is rolled over the samples (10, 20, 30, and 40 times). The peeling rate was varied at 1, 5,

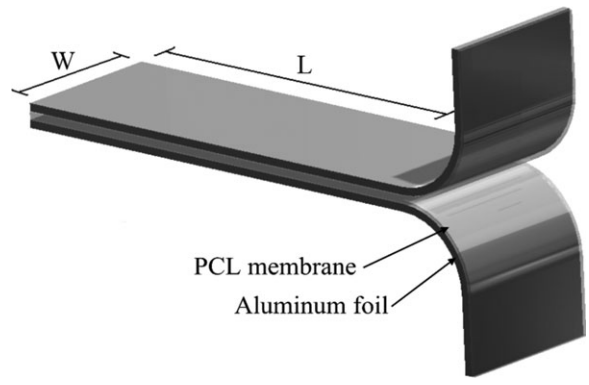

FIG. 3. Schematic drawing of the peel sample; $w = 0.5$ cm; $L = 4.5$ cm.

10, and 15 mm/min. All the tests are performed immediately after the pressure application.

Equation 1 is used to calculate the adhesive strength between the electrospun membranes.

$$G_t[\mathrm{Pa}] = \frac{\left(\frac{2 \cdot F}{W}\right)}{t} \quad (1)$$

where, F is the peel force, W the sample width, and t sample thickness, respectively. The sample thickness is measured by SEM.

Traditional adhesion strength values do not take into account sample thickness; this is because at a thickness greater than a threshold value this variable does not affect the adhesion strength. However, for very thin samples, in the scale relevant to our tests, there is a linear dependency on thickness [36, 42, 43]. Our peeling force results are clearly influenced by the membrane thickness, i.e., a doubling of membrane thickness produces a doubling of peel force. Therefore, for comparison purposes, the standard adhesive strength formula (G) is normalized by the membrane thickness (G_t), as it is explicit in *Eq. 1*.

Plastic yielding of adhesives may occur during the peel test. Plastic yielding is not taken into account in the adhesion strength calculations because: (1) the thickness is small and (2) the bending forces are negligible. Gent and Hamed [36] showed that even though very thin substrates will undergo complete plastic yielding on detachment, the total energy dissipated in this way will be small because the thickness (t) is small. Hence, additional peel force will be minor. Also, the influence of the substrates' plastic yielding in the total adhesive strength will depend on the degree of the adhesive forces. For example, if the adhesive forces are not high enough to generate a bending force responsible for yielding in the substrate, no rise in the adhesive strength will be obtained from yielding [37].

Statistical Analysis

All data are expressed as arithmetic means ± standard deviations. A T-test was used to compare adhesion strength between oriented and non-oriented membranes, with $P < 0.05$ as the measure for statistical significance.

RESULTS AND DISCUSSION

Electrospinning

Well-aligned fibrous membranes are obtained by using a tip collector as an electrospinning setup. According to Rafique et al. [41, 44, 45], the fibers are electrospun one by one. This occurs when the solution reaches a critical concentration, with a viscosity such that the needle ejects one fiber at a time. If this concentration is not reached, the fibers will be continuous and randomly oriented. Once the first fiber has reached the tip collector and is deposited on the plate collector, the next fiber will be deposited parallel to the previous one. The electrostatic charge of the already deposited fiber repels the charge of the incoming fiber. Thus, an aligned fibrous structure can be produced.

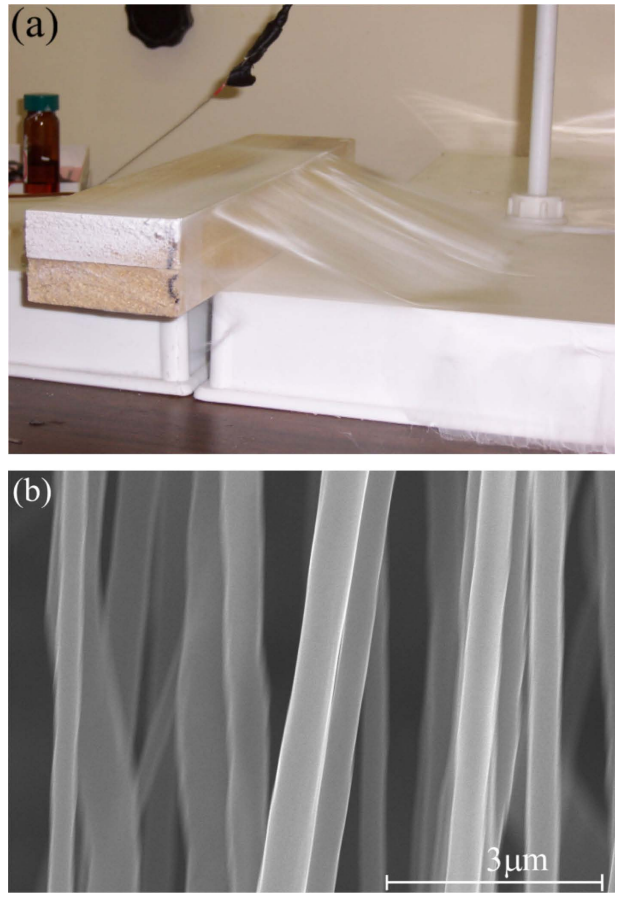

FIG. 4. (a) Macroscopic image of well aligned fibrous PCL membrane collected on the tip collector setup. (b) SEM micrograph of the A14DT membrane (V = 20 kV, L = 12 cm, $h1$ = 3.5 cm, $h2$ = 5.5 cm). [Color figure can be viewed in the online issue, which is available at wileyonlinelibrary.com.]

The critical concentration for PCL is reached at 14% wt/vol (A14DT). For lower concentrations, a non-fibrous or a random fibrous structure is obtained instead. Figure 4 shows (a) the macroscopic morphology of the electrospun membrane and (b) the microscopic morphology of the well-aligned PCL fibers.

The use of the A14DT solution (Fig. 5) produces a membrane with a mean fiber diameter of 486 ± 143 nm. The corresponding fiber diameter distribution (Fig. 5b) exhibits a narrow bell shaped pattern, which indicates the dominance of one fiber size in the sample. The nanofiber orientation is 95 ± 5.8°. The small standard deviation indicates that the fiber alignment is good; the corresponding fiber angle distribution is shown in Fig. 5c and it has a narrow bell shaped pattern.

In order to compare the adhesion properties between random and aligned electrospun membranes, a similar mean fiber diameter is needed to assure that the difference

 DOI 10.1002/pen

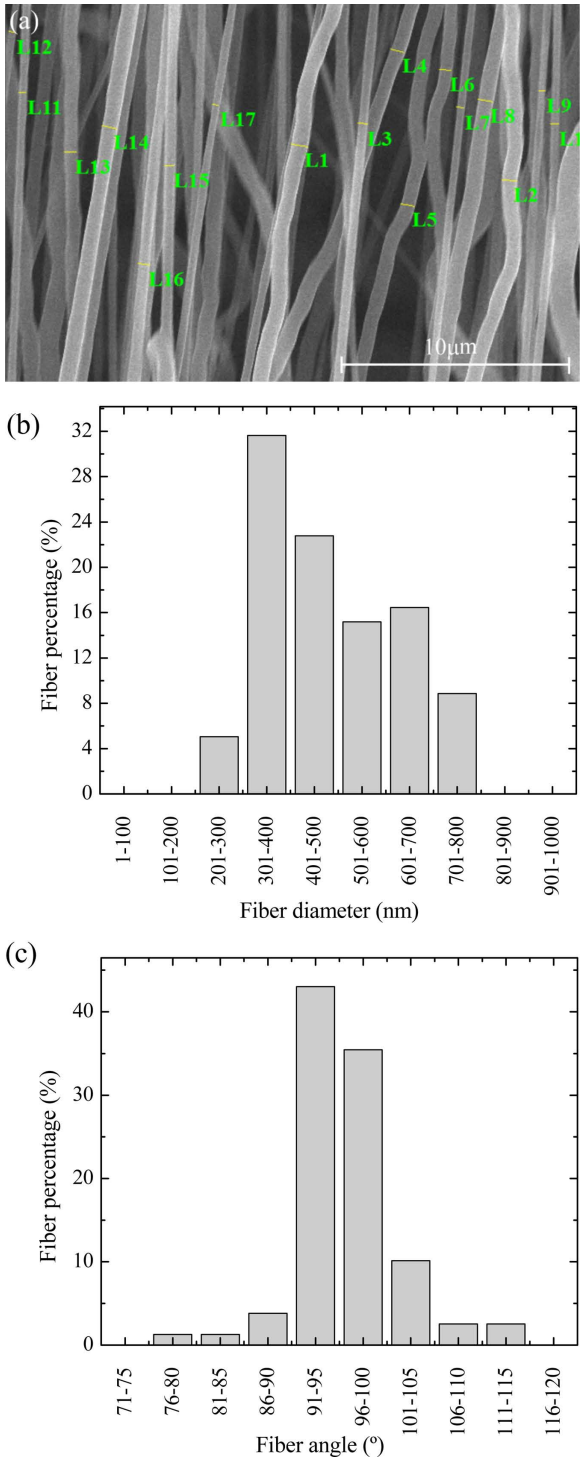

FIG. 5. (a) SEM micrograph of the A14DT membrane (V = 20 kV, L = 12 cm, $h1$ = 3.5 cm, $h2$ = 5.5 cm), (b) fiber diameter distribution, and (c) fiber angle distribution. [Color figure can be viewed in the online issue, which is available at wileyonlinelibrary.com.]

in the adhesive strength values is only influenced by fiber orientation. Therefore, a mean diameter of approximately 500 nm is desired for the random mat.

Many different solutions are attempted across trials and some bead-like structures could be seen. Three of these PCL solutions (R12DD, R13DD, and R13DT) produced a bead-free nanofiber structure. The mean fiber diameters are (i) 527 ± 237 nm for the R13DT solution, (ii) 563 ± 212 nm for the R12DD solution, and (iii) 578 ± 280 nm for R13DD solution. Although, the use of R13DT solution produces a membrane with a mean fiber diameter similar to the aligned membrane, the diameter histogram shows the presence of fibers of 1.7 μm and a dual fiber size population is observed by SEM. The membrane chosen for the adhesion characterization is obtained from the R12DD solution (Fig. 6), which presents a 563 nm mean fiber diameter and a small standard deviation. The diameter distribution presents a narrowed bell shaped pattern.

Peel Test

Aligned nanofibrous membranes peeling curves are shown in Fig. 7. An initial increase in load at crack opening, then a decrease in load as the detachment starts, and a final constant load zone during stable peel is observed. In some samples, an increase in the load at the end of the test could be observed, which was attributed to a border effect. This effect can be explained by the glue used to adhere the nanofibrous membranes to the aluminum foil. In some cases, the glue adheres the two membranes together, which causes an increase in load after the whole sample has completely peeled off. The average peel force, measured in the stable peel zone, does not include this artifact.

A positive, non-zero adhesive force is measured for the T-peel test between the nanofibrous membranes. The adhesion between the nanofibrous membrane and the aluminum foil, and between the aluminum foils, is measured to verify that the adhesive force is due only to the surface asperities in the PCL membrane. No adhesion to the aluminum foil is obtained.

The adhesive strength calculated by *Eq. 1* is 758.7 ± 211.7 kPa. Table 2 presents the effect of the peel rate (r) and the applied pressure (P) on the adhesive strengths of the aligned membranes. There is no significant change with the variables studied. Hence, it appears that the adhesion magnitude is affected primarily by the membranes' topology.

A lower adhesive strength value, 613.1 ± 79.9 kPa ($P < 0.05$), is obtained for random nanofibrous membranes. Moreover, Fig. 8 shows that the adhesive strength of the random membrane is lower than the values obtained from the different samples of aligned membranes. These findings provide additional evidence that membrane's surface asperities and their geometric arrangement are contributing to the adhesion properties. Recently, Wong and coworkers [10] showed that films with nanoscale topology obtained by electrospinning exhibit 10 times greater adhesion with respect to smooth cast films, due to high surface to volume ratio. The aligned nanofibers present a high aspect ratio band-like structure, which is ideal for synthetic dry adhesives [21]. The random mat, nevertheless, also presents high aspect ratio nanofibers, but their

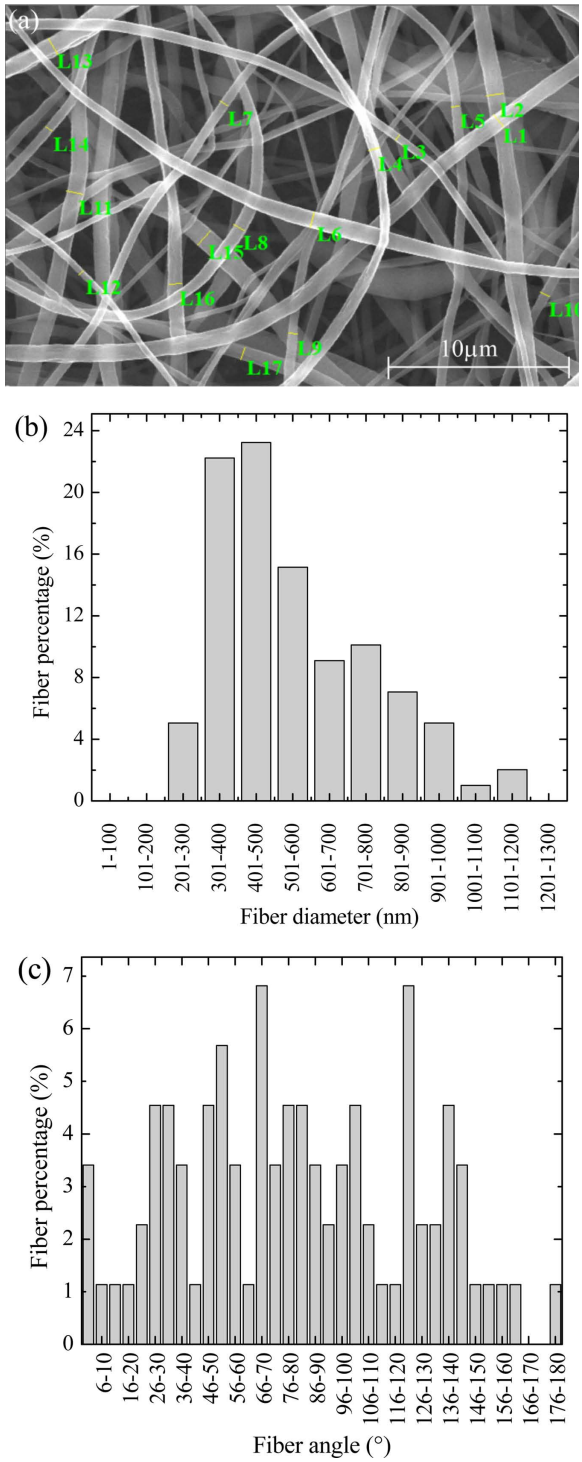

FIG. 6. (a) SEM micrograph of the R12DD membrane (V = 12 kV, d = 15 cm), (b) fiber diameter distribution, and (c) fiber angle distribution. [Color figure can be viewed in the online issue, which is available at wileyonlinelibrary.com.]

arrangement results in fewer contact points, decreasing the adhesive strength.

Nanofibers naturally adhere due to vdW forces [11, 29]. JKR contact mechanics model [46] allows estimation of one single-contact adhesion energy. In order to apply

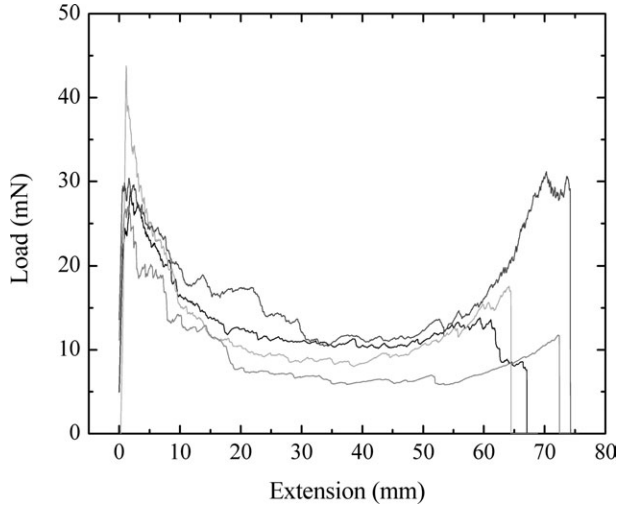

FIG. 7. Peel curves of aligned nanofibrous membranes for an applied pressure by ten times of rolling with a cylinder, a peel rate of 5 mm/min and a dwell time of zero.

the JKR force equation to our experimental data, we followed the Arzt equation [12].

$$P = \frac{3}{4} \cdot n \cdot \pi \cdot \gamma \cdot d \tag{2}$$

where P is the peel force, n the number of contacts, γ the adhesion energy of a single contact, and d the fiber diameter.

The Arzt paper extends the JKR equation to the case of adhesion by multiple contact points. The contact splitting phenomenon is considered. We assumed the validity of self-similar scaling principles. The number of contacts (nanofibers) (n) is approximated as the sample width is divided by the fiber diameter. Peel force is used as the adhesion force, which represents the adhesion between the membranes equal to pull-off force in the JKR model. The contact of the two parallel cylinders is assumed equal to contacts between two spheres as stated before [47].

From the application of *Eq. 2* to our data, a single contact adhesion energy of 83.1 ± 32.5 mJ/m^2 emerges. This value is within the order of magnitude of typical adhesion

TABLE 2. Adhesive strength values for different peel rates and applied pressures for the A14DT solution. Membrane thickness was measured after testing.

Peel rate (mm/min)	Applied pressure (replicates)	Peel force (mN)	Membrane thickness (μm)	Adhesive strength (kPa)	Standard deviation (kPa)
1	10	15.1	7.5	800.9	160.1
5	10	16.5	7.5	877.5	199.8
10	10	9.9	4.6	870.6	222.9
15	10	10.1	4.6	885.6	194.4
10	20	7.4	4.6	650.8	203.2
10	30	9.9	4.6	868.3	202.3
10	40	11.2	4.6	989.3	189.9

DOI 10.1002/pen

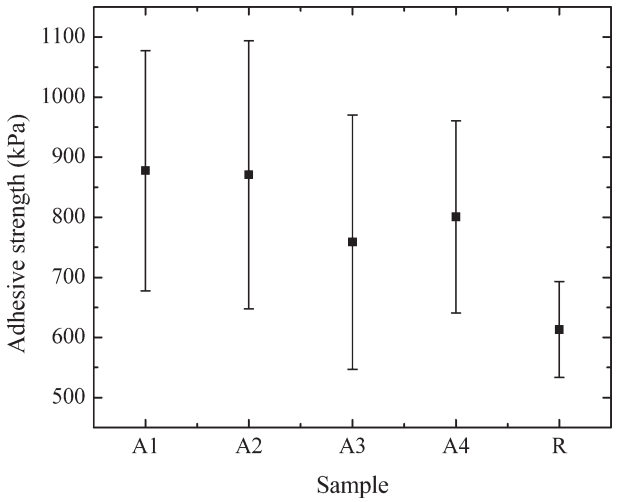

FIG. 8. Adhesive strength for aligned and random membranes. A1: aligned ($r = 5$ mm/min, $P = 10$, e1), A2: aligned ($r = 10$ mm/min, $P = 10$), A3: aligned ($r = 5$ mm/min, $P = 10$, e2), A4: aligned ($r = 1$ mm/min, $P = 10$), and R: random ($r = 5$ mm/min, $P = 10$).

energy reported for vdW force range (50–60 mJ/m^2) [3, 12], which suggests that vdW provides the dominant adhesion mechanism for electrospun PCL.

Adsorption theory states that the materials will adhere due to interatomic and intermolecular forces [37]. These include secondary bonds (vdW forces and hydrogen bond), primary bonds (ionic, covalent, and metallic), and donor–acceptor bonds.

The thermodynamic work of adhesion according to adsorption theory is, without taking into account the primary bonds:

$$W_a = 2 \cdot \left(\gamma^{AD} \cdot \gamma^{BD}\right)^{1/2} - k_5 \cdot \left(C^A \cdot C^B + E^A \cdot E^B\right) \cdot n^{AB} + W_A^P \quad (3)$$

where the acid–base interaction of work of adhesion is:

$$W_A^{AB} = -k_5 \cdot \left(C^A \cdot C^B + E^A \cdot E^B\right) \cdot n^{AB} \quad (4)$$

and W_A^p is the thermodynamic work of adhesion arising from dipole–dipole interactions (which are usually negligible).

So if vdW forces are the predominant mechanism of adhesion, the single contact adhesion energy (calculated by JKR-model) should match the input from the dispersion thermodynamic work of adhesion. γ^D for PCL was measured by Cava et al. [48], obtaining a value close to 40 mJ/m^2. They also showed that the acid–base character of PCL surface is small, defining its interface as neutral. Taking these factors into account, we obtain from *Eq. 3* a value of $W_a = 80$ mJ/m^2, where only the secondary bond input is relevant. This value is in excellent agreement with the calculated single-fiber-contact adhesion energy of 83.1 ± 32.5 mJ/m^2, which suggests vdW forces are the primary mechanism of adhesion between electrospun nanofibers.

The structure of tested samples is analyzed by SEM. As shown in Fig. 9, no permanent deformation is observed in the micrographs, both aligned and random mats present equivalent structures to those observed before they are tested. The micrographs show no sign of cohesive fracture or plastic deformation, while the structural integrity of the samples is preserved. Furthermore, a non-negligible adhesion force value is detected. It can be concluded that the adhesion between the membranes is due to interactions in agreement with vdW forces.

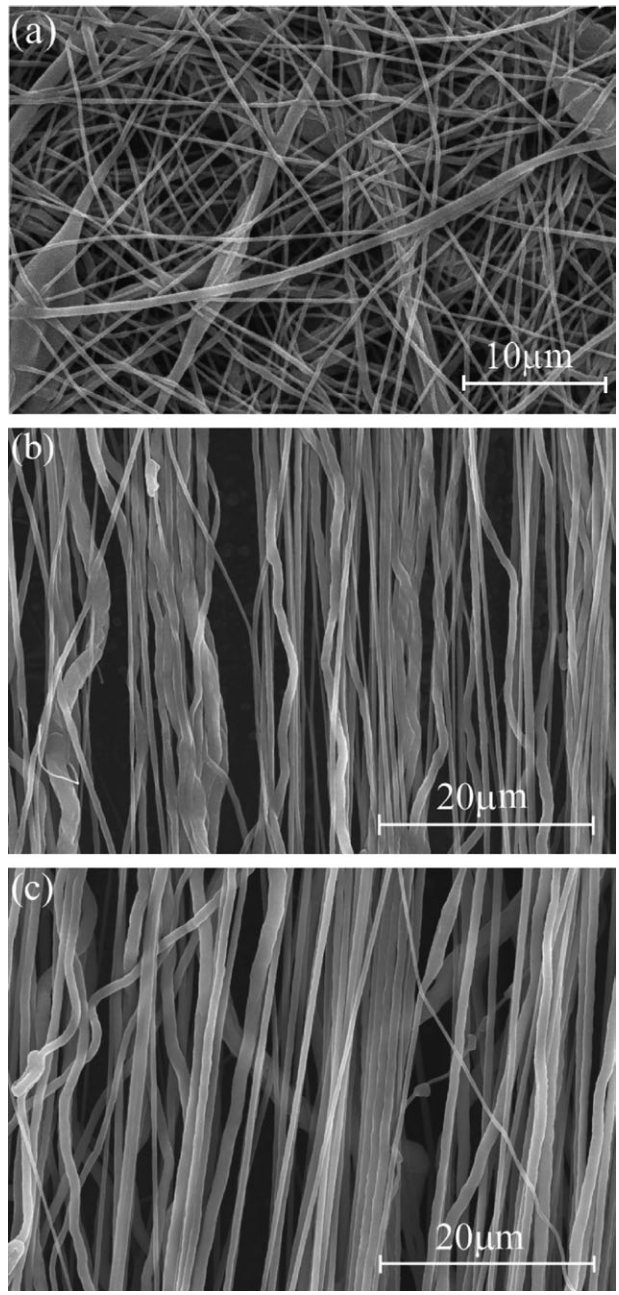

FIG. 9. SEM micrographs of the PCL nanofibrous membranes after the T-peel test is carried out: (a) random membranes, (b) aligned membranes at the beginning of the test, and (c) at the stable load zone.

CONCLUSIONS

The adhesive strength between aligned and random nanofibrous mats was successfully compared using a T-peel test configuration. The energy values indicated that the nanofibrous hydrophobic membranes presented surface asperities that contributed to enhanced adhesion. The influence of the orientation of the nanofibers on the adhesive strength was also evaluated. Well-aligned structure enhanced adhesion by introducing more contact points than in the case with a random mat. Adhesion between nanofibers was due to interactions in the nanometer range, since neither plastic deformation nor interlocking was observed. The single contact adhesion energy value calculated using JKR contact mechanics and the adsorption theory analysis suggested that vdW forces provided the primary adhesion mechanism. This study demonstrated how a change in surface topology can readily increase the adhesive strength of fibrous membranes, a principle seen in natural dry adhesive structures such as insect tarsal pads and gecko toes and which could be applied to a variety of synthetic electrospun materials.

ACKNOWLEDGMENTS

The authors pay tribute to the late Prof. Alan Gent for advising on the peel testing procedures. Provision of Fig. 1 from Johnny F. Najem's PhD Dissertation [24] at the University of Akron under the direction of one of us (SCW) is acknowledged. Assistance from Dr. H. Na, who is presently at the Ningbo Institute of Materials Technology and Engineering, with preparing this manuscript, is appreciated.

REFERENCES

1. M.A. Meyers, P.Y. Chen, M.I. Lopez, Y. Seki, and A.Y.M. Lin, *J. Mech. Behav. Biomed. Mater.*, **4**, 626 (2011).
2. P. Fratzl, *J. R. Soc. Interface*, **4**, 637 (2007).
3. K. Autumn, M. Sitti, Y.A. Liang, A.M. Peattie, W.R. Hansen, S. Sponberg, T.W. Kenny, R. Fearing, J.N. Israelachvili, and R.J. Full, *Proc. Natl. Acad. Sci. USA*, **99**, 12252 (2002).
4. K. Autumn, Y.A. Liang, S.T. Hsieh, W. Zesch, W-P Chan, T.W. Kenny, R. Fearing, and R.J. Full, *Nature*, **405**, 681 (2000).
5. C. Greiner, A. del Campo, and E. Arzt, *Langmuir*, **23**, 3495 (2007).
6. A.K. Geim, S.V. Dubonos, I.V. Grigorieva, K.S. Novoselov, A.A. Zhukov, and S.Y. Shapoval, *Nat. Mater.*, **2**, 461 (2003).
7. M.P. Murphy, S. Kim, and M. Sitti, *ACS Appl. Mater. Interfaces*, **1**, 849 (2009).
8. S. Sethi, L. Ge, L. Ci, P.M. Ajayan, and A. Dhinojwala, *Nano Lett.*, **8**, 822 (2008).
9. L. Ge, S. Sethi, L. Ci, P.M. Ajayan, and A. Dhinojwala, *Proc. Natl. Acad. Sci. USA*, **104**, 10792 (2007).
10. H. Na, P. Chen, K.T. Wan, S.C. Wong, Q. Li, and Z. Ma, *Langmuir*, **28**, 6677 (2012).
11. Q. Shi, K.T. Wan, S.C. Wong, P. Chen, and T.A. Blackledge, *Langmuir*, **26**, 14188 (2010).
12. E. Arzt, S. Gorb, and R. Spolenak, *Proc. Natl. Acad. Sci. USA*, **100**, 10603 (2003).
13. K. Autumn and A.M. Peattie, *Integr. Comp. Biol.*, **42**, 1081 (2002).
14. A. Peressadko and S.N. Gorb, *J. Adhes.*, **80**, 247 (2004).
15. H. Parsaiyan, F. Barazandeh, S.M. Rezaei, M. Parsaiyan, and M. Safdari, *Int. J. Adhes. Adhes.*, **29**, 444 (2009).
16. S. Chen and H. Gao, *J. Mech. Phys. Solids*, **55**, 1001 (2007).
17. H. Yao, S. Chen, P.R. Guduru, and H. Gao, *Int. J. Solids Struct.*, **46**, 1167 (2009).
18. R. Spolenak, S. Gorb, H. Gao, and E. Arzt, *Proc. R. Soc. A*, **461**, 305 (2005).
19. C. Greiner, R. Spolenak, and E. Arzt, *Acta Biomater.*, **5**, 597 (2009).
20. H. Gao and H. Yao, *Proc. Natl. Acad. Sci. USA*, **101**, 7851 (2004).
21. C. Greiner, Size and Shape Effects in Bioinspired Fibrillar Adhesives, PhD dissertation, University of Stuttgart (2007).
22. Y. Dzenis, *Science*, **304**, 1917 (2004).
23. D.H. Reneker, A.L. Yarin, E. Zussman, and H. Xu, "Electrospinning of Nanofibers from Polymer Solutions and Melts," in *Advances in Applied Mechanics Vol 41,* H. Aref, E. van der Giessen (ed), Academic Press, Waltham, Massachusetts, **43** (2007).
24. J.F. Najem. *Gecko-Inspired Electrospun Fiber Arrays for Adhesion*, PhD Dissertation, University of Akron (2012).
25. A. Baji, Y.W. Mai, S.C. Wong, M. Abtahi, and P. Chen, *Compos. Sci. Technol.*, **70**, 703 (2010).
26. S.C. Wong, A. Baji, and S.W. Leng, *Polymer*, **49**, 4713 (2008).
27. A.L. Yarin and E. Zussman, *Polymer*, **45**, 2977 (2004).
28. W.E. Teo and S. Ramakrishna, *Nanotechnology*, **17**, R89 (2006).
29. X. Wang, J.F. Najem, S.V. Wong, and K.T. Wan, *J. Appl. Phys.*, **111**, 024315–1 (2012).
30. M.A. Woodruff and D.E. Hutmacher, *Prog. Polym. Sci.*, **35**, 1217 (2010).
31. A.C. Albertsson and I.K. Varma, "Aliphatic Polyesters: Synthesis, Properties and Applications," in *Advances in Polymer Science, vol. 157*, A. Abe, A.C. Albertsson, H.J. Cantow, K. Dusek, S. Edwards, H. Hocker, J.F. Joanny, H.H. Kausch, K.S. Lee, J.E. McGrath, L. Monnerie, S.I. Stupp, U.W. Suter, G. Wegner, and R.J. Young, Eds., Springer, Berlin, Heidelberg, **1** (2002).
32. W.F. Busse, J.M. Lambert, and R.B. Verdery, *J. Appl. Phys.*, **17**, 376 (1946).
33. T. Hata, *Kobunshi Kagaku*, **4**, 67 (1947).
34. J.J. Bikerman, *J. Appl. Polym. Sci.*, **2**, 216 (1959).
35. J.J. Bikerman, *J. Appl. Phys.*, **28**, 1484 (1957).
36. A.N. Gent and G.R. Hamed, *Polym. Eng. Sci.*, **17**, 462 (1977).
37. A.J. Kinloch, *Adhesion and Adhesives: Science and Technology*, Chapman and Hall, London, New York, Tokyo, Melbourne, Madras (1990).
38. J.L. Gardon, *J. Appl. Polym. Sci.*, **7**, 625 (1963).
39. J.L. Gardon, *J. Appl. Polym. Sci.*, **7**, 643 (1963).
40. D.H. Kaelble, *Trans. Soc. Rheol.*, **3**, 161 (1959).

41. J. Rafique, J. Yu, J. Yu, G. Fang, K.W. Wong, Z. Zheng, H.C. Ong, and W.M. Lau, *Appl. Phys. Lett*., **91**, 063126–1 (2007).
42. Y. Wei and J.W. Hutchinson, *Int. J. Fract*., **93**, 315 (1998).
43. Y. Wei, *Int. J. Solids Struct*., **41**, 5087 (2004).
44. J. Yu, Y. Qiu, X. Zha, M. Yu, J. Yu, J. Rafique, and J. Yin, *Eur. Polym. J*., **44**, 2838 (2008).
45. Y. Qiu, J. Yu, J. Rafique, J. Yin, X. Bai, and E. Wang, *J. Phys. Chem. C*, **113**, 11228 (2009).
46. K.L. Johnson, K. Kendall, and A.D. Roberts, *Proc. R. Soc. Lond. A*, **324**, 301 (1971).
47. V.L. Popov, "Rigorous Treatment of Contact Problems–Hertzian Contact," in *Contact Mechanics and Friction: Physical Principles and Applications,* Springer-Verlag, Berlin, Heidelberg, **55** (2010).
48. D. Cava, R. Gavara, J.M. Lagarón, A. Voelkel. J. *Chromatogr. A*, **1148**, 86 (2007).